coatings

MDPI

Article

Controlled Compositions in Zn–Ni Coatings by Anode Material Selection for Replacing Cadmium

Lijia Yi *, Shuncai Wang and Robert J. K. Wood

National Centre for Advanced Tribology, Department of Mechanical Engineering, University of Southampton, Southampton SO17 1BJ, UK; wangs@soton.ac.uk (S.W.); r.wood@soton.ac.uk (R.J.K.W.)
* Correspondence: ly1d19@soton.ac.uk

Abstract: Cadmium-based coatings have long been used to protect high-strength steel in aerospace, but due to cadmium's toxic and carcinogenic nature, its use is increasingly restricted. Zinc–nickel coatings, containing 10–14 wt% Ni, offer superior corrosion resistance compared to pure zinc, making them a promising alternative. However, Zn–Ni coatings are prone to cracking, which can compromise their protection. This study investigates how different anode materials influence crack formation and coating properties during electrodeposition. Zinc and nickel anodes produced coatings with consistent thicknesses of 13–15 µm, while 1020 steel and stainless steel resulted in thicker coatings of up to 33 µm. Notably, coatings deposited with nickel anodes demonstrated strong adhesion and consistent interface quality. Zinc anodes achieved a high Ni content of about 13.5 wt%, whereas 1020 steel and stainless steel produced lower Ni content, around 7 wt%. Additionally, zinc and nickel anodes led to fewer defects and minimal porosity, in contrast to the higher porosity observed with 1020 steel and stainless steel anodes. Furthermore, zinc anodes maintained stable voltages (~0.5 V), contributing to more uniform coatings. In terms of corrosion resistance, zinc anodes exhibited a lower corrosion rate of 0.44 mm/year compared to 1.54 mm/year for nickel anodes. This study highlights the importance of anode selection in reducing cracking and optimizing Zn–Ni coatings, presenting them as a safer and more effective alternative to cadmium-based coatings.

Keywords: Zn–Ni coatings; phase composition; XRD analysis; electrodeposition; anode material

Citation: Yi, L.; Wang, S.; Wood, R.J.K. Controlled Compositions in Zn–Ni Coatings by Anode Material Selection for Replacing Cadmium. *Coatings* **2024**, *14*, 1119. https://doi.org/10.3390/coatings14091119

Academic Editors: Rongguang Wang, Her-Hsiung Huang and Jiaqian Qin

Received: 25 July 2024
Revised: 29 August 2024
Accepted: 30 August 2024
Published: 2 September 2024

1. Introduction

Cadmium coatings have long been employed to significantly enhance the corrosion resistance of a variety of materials, making them essential for a broad range of components and parts used in many industrial applications. The application of cadmium coatings has been particularly common in industries where maintaining the integrity of steel components is critical [1]. High-strength steel fasteners used in automotive and aerospace industries are often coated with Zn- or Cd-based coatings for anodic protection [2]. However, despite the advantageous properties that make cadmium an effective protective coating, its use has become increasingly contentious. The primary concerns come from cadmium's carcinogenic and toxic nature, which poses significant health risks to workers as well as environmental hazards [3,4]. Despite its extensive use as a coating for steel, cadmium's carcinogenic and toxic nature has raised significant health and environmental concerns, leading to increased restrictions on its use [5].

Electroplated zinc has provided an economical and highly corrosion-resistant coating. However, conventional zinc electroplates are increasingly being replaced by zinc alloys [6]. Zn alloy coatings are extensively used to protect steel components across various industries, including automotive, electrical, construction, aerospace, and fasteners [7]. They are obtained by alloying Zn with more noble metals in the Fe group such as Ni, Co, Sn, and Fe. The addition of these elements alters the corrosion rate and potential. Zn–Ni alloys offer the greatest reduction in corrosion rate and the most significant positive shift in corrosion

potential, followed closely by Zn–Co alloys. Zn–Sn and Zn–Fe alloys also enhance corrosion resistance but to a lesser degree. The degree of improvement typically increases with the concentration of the alloying metal, particularly for Ni and Co. Overall, the trend in effectiveness is generally Ni > Co > Sn > Fe for reducing corrosion rates and enhancing corrosion potential [8–14]. Zinc-based alloys maintain their anodic behaviour to steel, ensuring sacrificial protection while offering a lower corrosion rate, thereby providing longer-lasting corrosion protection [15].

For decades, Zn–Ni coatings have attracted much attention because they possess higher corrosion resistance and better mechanical characteristics than zinc and other zinc alloy coatings [6,16] and have become a widely used, eco-friendly alternative to toxic cadmium coatings [17]. It has been reported that Zn–Ni coatings with Ni content in the range of 10–14 wt% have shown five times better corrosion resistance compared to pure Zn [18–21]. It has been studied by Mosavat et al. [22] that Ni content plays a significant role in the corrosion resistance of deposits. Twelve wt% Zi–Ni coatings had the highest hardness and corrosion resistance among all the alloy coatings while Gnanamuthua et al. [23] investigated the structure, hardness, and corrosion properties of Zn–Ni coatings on AISI 347 steel substrates. Conde et al. [20] revealed that when Ni content has a higher concentration, exceeding 25–30 wt%, the corrosion resistance of the coating relies only on the barrier properties of the alloy and is no longer sacrificial with respect to the steel substrate.

Significant research has been carried out to understand the characteristics of the electrodeposition process of Zn–Ni alloys [24]. It was found that the features of the deposited coatings are highly dependent on the bath composition, current density, pH, applied voltage, additives, and temperature, as well as the phases and crystal structure.

The use of saccharin as an additive has played a significant role in improving surface homogeneity and grain size. The study of the microstructure has shown brighter coatings when saccharin is added to the Zn–Ni electrodeposition bath [25]. It has been found that the addition of saccharin to the electrolyte could decrease the surface roughness and the crystallite size in electrodeposited Zn–Ni alloy films by Mosavat et al. [6] and that it works as a 'carrier', which is the most effective internal stress reducer and often helps to decrease or eliminate hazes of the deposit [26].

Zn–Ni coatings have attracted significant attention due to their superior properties compared to Cd coatings. Notably, whereas Cd coatings typically last around 1000–1200 h in a salt spray test (ASTM B117), Zn–Ni coatings with the same thickness as the Cd coatings exhibit exceptional corrosion resistance that lasts four times longer than cadmium in salt spray [27]. Additionally, Zn–Ni coatings offer high mechanical strength, being significantly harder and more wear-resistant than Cd coatings [2]. These advantages have driven extensive research and development efforts in recent years to further optimise Zn–Ni coatings across various applications. People have been studying Zn–Ni electrodeposits from varying conditions, such as the choice of using different anode materials. Thangaraj et al. [28], for example, investigated the compositional behaviour of Zn–Ni alloy using a pure zinc anode in a sulphate bath. It was concluded that not only does the corrosion resistance of the coating depend on the wt% Ni in the deposits but also it depends on their morphology. Farooq et al. [17] conducted electrodeposition using a nickel anode in an acid sulphate bath with varying concentrations of Ni in the electroplating bath. It was suggested that dissolution characteristics of the Zn–Ni alloy coating can be effectively tuned by varying the Ni^{2+} concentration in the bath solution. Some experiments were undertaken by using stainless steel as anode. Tafreshi et al. [29] used a 316L stainless steel plate as anode material to deposit the Zn–Ni and Zn–Ni/PTFE coatings and indicated that the wear resistance of a Zn–Ni/PTFE composite electrodeposit is about 1.5 times better than the cadmium coating when conducting dry sliding pin-on-disc wear tests using AISI 52100 steel pins (5 mm diameter, 64 HRC) at room temperature with a 2 N load, 200 m sliding distance, and 0.1 m/s speed.

As seen from the above literature, experimental studies have been implemented on Zn–Ni deposition using Zn, Ni, and stainless steel anodes. To the best of the authors'

knowledge, there has not been a systematic study that specifically compares the quality and performance of Zn–Ni alloys deposited using different anodes. Therefore, this present research is directed at investigating and analysing the Zn–Ni alloy deposited under various conditions with the use of different anode materials.

2. Experimental

AISI 1020 steel sheets with exposed areas of 6 cm^2 were used as cathodes. The chemical composition of the 1020 steel is 0.17–0.23 wt% C, 0.22 wt% Si, 0.4 wt% Mg, <0.04 wt% P, <0.05 wt% S, and 99.08–99.53 wt% Fe. Before electrodeposition, each substrate was ground with emery papers (grades: 120, 800, 1000, 4000) to achieve a roughness Ra of 0.05 µm. Afterwards, the substrates were placed in an acetone bath and treated with ultrasound for 5 min. Following this step, they were rinsed with distilled water and immediately immersed in an electroplating bath. Nickel, zinc, 1020 steel, and 316 L stainless steel sheets were used as anodes. After the electrodeposition process, the plated specimens were rinsed with distilled water and ethanol, followed by air drying.

The experiments were conducted using a two-electrode cell with a capacity of 100 mL. The electroplating bath was subjected to magnetic stirring for 1 h before use, and the pH was adjusted by adding H_2SO_4 (10 vol%) from 4.3 to 3.

The optimised bath composition and plating parameters are presented in Table 1.

Table 1. The composition of the electroplating bath and plating parameters.

Bath Components	Composition
$ZnSO_4 \cdot 7H_2O$	90 g/L
$NiSO_4 \cdot 7H_2O$	170 g/L
Na_2SO_4	80 g/L
H_3BO_3	40 g/L
$NaCl_2H_{25}SO_4$ (SDS)	0.1 g/L
Saccharin	2 g/L
Plating Parameters	
Current Density	4 A/dm^2
pH	3
Temperature	60 °C
Time	20 min
Rotation Speed	350 rpm

For the corrosion studies, electrochemical measurements were performed in a three-electrode cell using an Ag/AgCl electrode as the reference electrode and a platinum counter electrode using an Autolab PGSTAT302N potentiostat. All the corrosion tests were carried out in a 3.5 wt% NaCl solution. Different types of electrochemical tests were used to evaluate the sacrificial and barrier properties, as well as the corrosion kinetics of the coatings such as polarisation curves, measurement of the open circuit potential (OCP), and measurement of the mixed potential (E_{corr}) and galvanic current density (i_{corr}) in coupled Zn–Ni coated/steel specimens.

Surface morphologies of the coatings were examined using a JSM7200F scanning electron microscope (SEM). Phase composition of the coatings was determined by X-ray diffraction (XRD) analysis using a diffractometer (model Rigaku SmartLab) with Cu Kα radiation (λ = 0.15405 nm). The 2θ ranged from 10° to 90° and the scan rate was 0.02 °/s. The average crystallite size of the coatings was determined from X-ray line broadening using Scherrer equation, as follows [30]:

$$D = \frac{K\lambda}{\beta \cos\theta} \quad (1)$$

where D is the average crystallite size, λ is the wavelength of the radiation, K is the shape factor or Scherrer constant, θ is the Bragg angle and β is the full width at the half maximum (FWHM).

The hardness of deposits was measured using a Vickers microhardness indenter under an applied load of 100 g for 15 s at room temperature. An average of five measurements were carried out on each coating.

3. Results and Discussion

3.1. Voltage Analysis

The voltage changes observed during direct current electrodeposition varied significantly with different anodes, prompting a detailed investigation into the effect of anode material on voltage behaviour and its impact on the quality and efficiency of Zn–Ni coatings. With the prospect of achieving a more compact growth of the layer, other coatings were also deposited at the same conditions with the aim of preserving the Ni content, but with different anodes of Zn, Ni, 1020 steel, and 316 L stainless steel. Figure 1 shows the variation of voltage over time for each type of anode used in the Zn–Ni coatings deposition. In the curves for Zn and 316 L stainless steel anodes, the voltage remains relatively stable over time with only minor fluctuations, and the Ni anode curve shows a stable trend with a very gradual decrease in voltage. The 1020 steel anode curve reveals a distinctive behaviour with a sharp initial voltage drop followed by stabilisation at a lower voltage, which could imply an inefficiency or different deposition dynamics in the initial stages of deposition. Zn, Ni, and 316 L stainless steel anodes provide more stable voltage trends, which indicate more consistent coating processes.

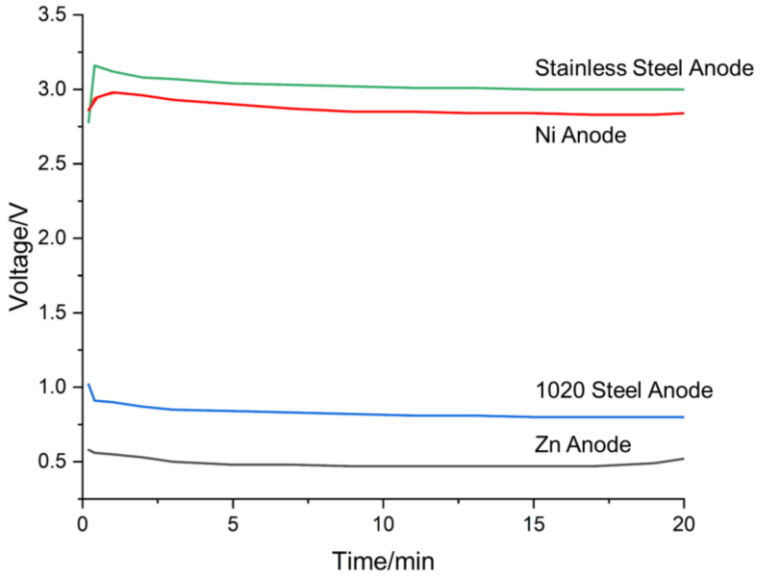

Figure 1. Voltage time for Zn–Ni coatings during electrodeposition process under 60 °C with a current density of 4 A/dm^2 with Zn, Ni, 1020 steel, and 316 L stainless steel anodes.

During the Zn–Ni electroplating process, the applied voltage drives the reduction of metal ions (Zn^{2+} and Ni^{2+}) from the electrolyte onto the cathode, forming the Zn–Ni alloy coating. The choice of anode material influences the overall cell potential needed to maintain a stable plating current.

The high and stable voltage indicates that the stainless steel anode offers little interference with the deposition process. The voltage remains high due to the higher overpotential required to sustain the cathodic reaction without significant anode dissolution or side reac-

tions. The stability of the voltage suggests efficient and consistent Zn–Ni deposition. The nickel anode also requires a high voltage, though slightly lower than stainless steel. This is because nickel can participate in the electrochemical reactions to some extent, reducing the overall energy required. The gradual voltage decrease could be due to the surface of the nickel anode becoming more active over time, leading to more efficient ion transfer, and slightly reducing the required voltage. The initial sharp drop with the 1020 steel anode in voltage indicates a high initial resistance, possibly due to surface oxidation or other reactions at the steel anode that temporarily hinder the process. This behaviour may also result from polarization effects, where the potential initially increases due to resistance at the electrode–electrolyte interface and then decreases as the system reaches a steady state. The unique properties of 1020 steel, such as its low carbon content (0.18%–0.23%) and relatively high surface reactivity, may influence its ionization process and initial interactions with the electrolyte. Additionally, the low carbon content makes 1020 steel less hard and more prone to forming a passivating oxide layer, which could explain the voltage drop. As these reactions stabilise, the voltage drops and remains low, suggesting that the 1020 steel anode might be less effective in maintaining the ideal conditions for Zn–Ni deposition, possibly due to side reactions or inefficiencies. The low voltage for the zinc anode suggests that it is more compatible with the Zn–Ni deposition process. Zinc readily dissolves into the electrolyte, which can directly contribute to the plating, reducing the required applied voltage. The slight fluctuations reflect the dynamic nature of zinc dissolution and redeposition.

In each electrodeposition process with different anodes used, the interaction between the anode material and the electrolyte influences the ion composition available for deposition at the mild steel cathode. Active anodes like zinc and nickel contribute directly to the electrolyte, supporting a more efficient and controlled deposition process. Inert or passivating anodes like stainless steel and 1020 steel may require higher voltages and could introduce challenges in maintaining consistent deposition quality, particularly if unwanted ions or passivation effects occur. The careful selection of anode material is crucial for optimizing the electroplating process and achieving the desired coating characteristics on the mild steel substrate.

3.2. Morphology

The Zn–Ni coatings obtained from the acid electrolyte bath showed a strong dependency of the morphology and composition on the deposition conditions of the coatings [31]. The morphology was obtained using SEM. For the as-deposited coatings, the samples were cleaned using acetone, followed by air drying at room temperature. For cross-sectional coatings, the samples were sectioned perpendicular to the coating surface using a diamond saw, and then embedded in epoxy resin. The cross-sections were polished with progressively finer abrasive papers and diamond suspension to achieve a smooth finish. Finally, for the anode plate materials, the plates were ultrasonically cleaned in acetone for 10 min and then air-dried.

The surface morphology of the Zn–Ni alloy coating electrodeposited using different anodes was investigated under a scanning electron microscope. The morphology of the deposited Zn–Ni alloy coating in terms of its uniformity, presence of porosity onto it, grain size, stress developed, etc., changes with the current density and bath composition.

In Figure 2a, the Zn anode results in a coating with a surface morphology characterised by fine platelets, each measuring less than 1 μm in size, suggesting a relatively smooth and homogeneous deposition. Conversely, the coating shown in Figure 2b, produced using a Ni anode, exhibits a rougher surface morphology with a granular and nodular appearance, indicative of larger particles and less uniform deposition. Figure 2c, representing the coating with a 1020 steel anode, reveals a significantly rough and uneven surface with an absence of distinct spherulitic formations, suggesting a less controlled deposition process and the formation of large, irregular clusters. Finally, in Figure 2d, the stainless steel anode produces a more organised surface structure with uniformly sized and shaped particles.

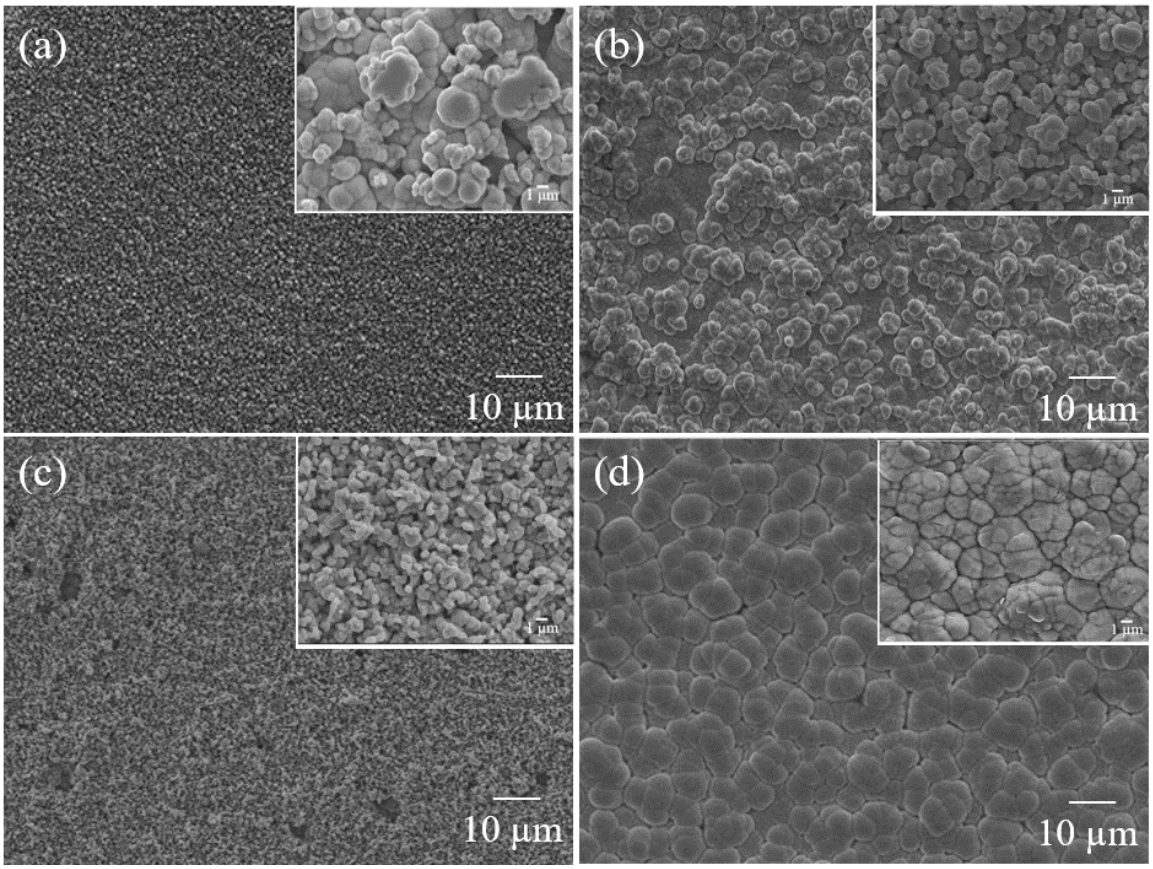

Figure 2. Surface morphologies of as-deposited Zn–Ni coatings using anode material of (**a**) Zn, (**b**) Ni, (**c**) 1020 steel, (**d**) stainless steel.

The study of the cross-sectional morphology of electrodeposited coatings is crucial for understanding the fundamental characteristics and performance of the coatings. Cross-sectional analysis provides detailed insights into the internal structure, thickness, uniformity, and adhesion of the deposited layers. Figure 3 shows the cross-section views for the Zn–Ni coatings using different anodes, and the thickness of the four cross-sectional Zn–Ni coatings is shown in Figure 4. The Zn–Ni coating using a Zn anode, as shown in Figure 3a, produces a coating around 14.5 µm thick with a uniform and fine-grained structure, exhibiting minimal porosity and good adhesion to the substrate; a Ni anode coating in Figure 3b results in a slightly thinner coating, around 12.8 µm, with similar minimal defects and good adhesion; using 1020 steel as the anode yields a thicker coating with some porosity and a coarser particle structure, indicating its potential for higher deposition rates but also increased porosity, as seen in Figure 3c; and, as can be seen from Figure 3d, the coating using 316 L stainless steel as the anode produces the thickest coating, but it has highest variability in measurements, with significant porosity, adhesion issues, and through-thickness cracks and very rough surface morphology. Therefore, resulting in better coating quality, the steel anodes, particularly 316 L stainless steel, may introduce impurities, alter the electrochemical environment, and disrupt the deposition process, leading to poor coating quality.

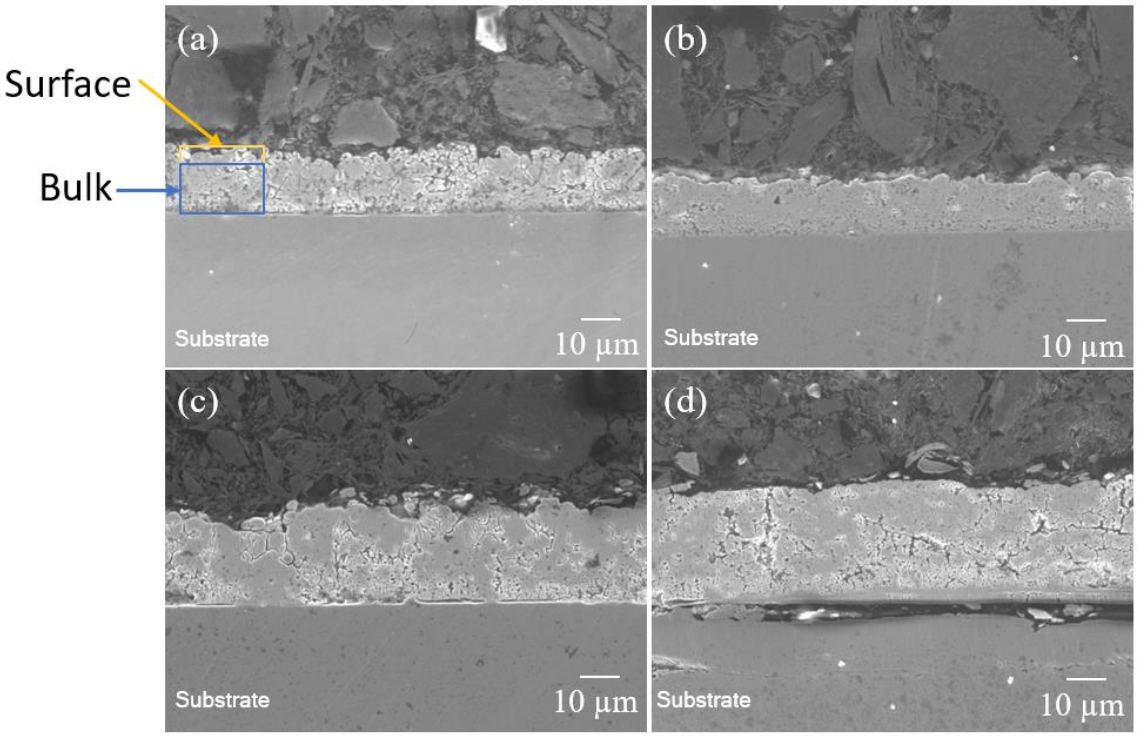

Figure 3. Cross-sectional morphologies of as-deposited Zn–Ni coatings using anode material of (**a**) Zn, (**b**) Ni, (**c**) 1020 steel, (**d**) stainless steel.

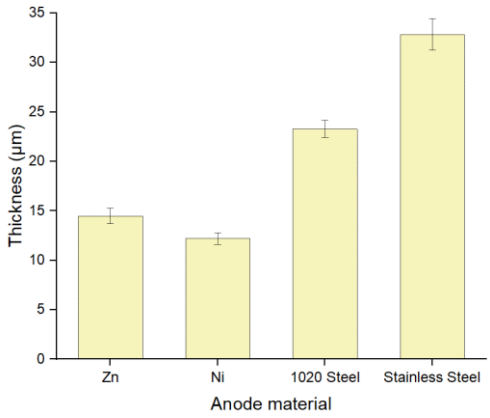

Figure 4. Thickness measured from cross-sectional morphologies of Zn–Ni coatings using different anodes.

The cross-sectional and surface morphologies demonstrate that the choice of anode material significantly impacts the quality of Zn–Ni alloy coatings. Zn and Ni anode coatings provide superior coatings with better density, uniformity, and adhesion, with a thickness of around 15 μm, which was also studied by Tian et al. [32] with a thickness of 15 μm for the Zn–Ni coatings. Notably, coatings deposited with a nickel anode exhibited superior interface characteristics, demonstrating strong adhesion to the substrate and consistent interface quality. While 1020 steel and 316 L stainless steel anode coatings suggest higher deposition rates as they are much thicker, with a thickness of 23 μm and 33 μm, respectively, they result in poor-quality coatings with significant defects and porosity. However, Tafreshi et al. [29] measured the thickness of the Zn–Ni coatings using 316 L stainless steel as the anode of around 20 μm.

The surface morphologies of anode materials before and after electrodeposition are shown in Figure 5, the surface morphology of the Zn anode changes from a relatively smooth texture before electrodeposition to a uniformly smooth surface after deposition,

indicating a successful and even coating. The Ni anode transitions from a smoother surface before electrodeposition to a surface with noticeable holes and increased roughness post-deposition. This change may be attributed to oxidation and the loss of Ni ions during the process, leading to the formation of voids and surface degradation. For the 1020 steel anode, the surface goes from being smooth with linear patterns before the deposition to a granular and crystallised structure afterwards, indicating substantial changes in the surface characteristics. The stainless steel anode, initially showing irregular features, develops distinct crystallographic patterns with sharp grain boundaries after electrodeposition, demonstrating a more structured and defined surface.

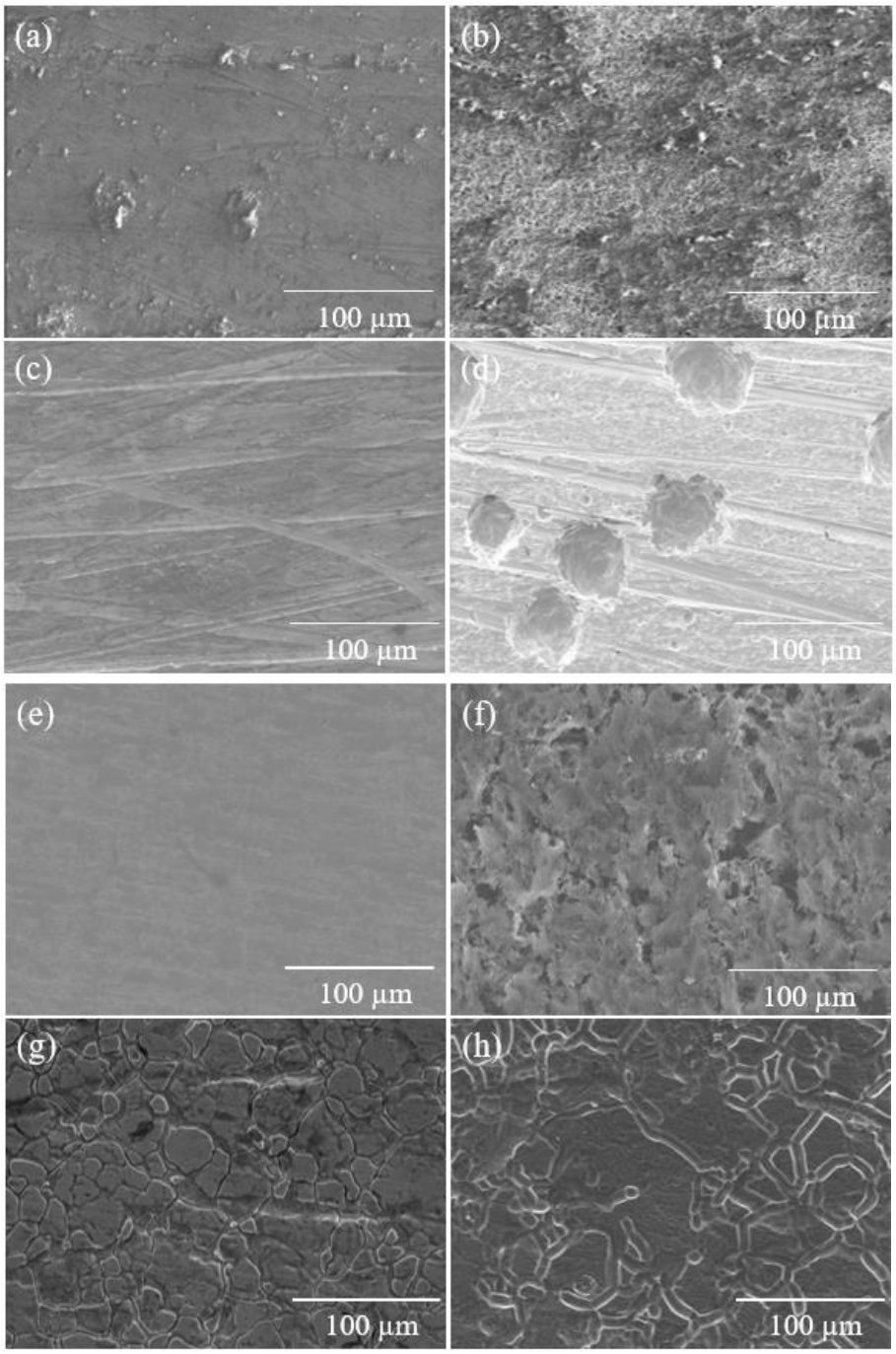

Figure 5. Surface morphologies of anode materials before electrodeposition: (**a**) Zn, (**b**) Ni, (**c**) 1020 steel, and (**d**) stainless steel; after electrodeposition: (**e**) Zn, (**f**) Ni, (**g**) 1020 steel, and (**h**) stainless steel.

3.3. Ni Concentration

As shown in Figure 6, the choice of anode material significantly affects the composition of the Zn–Ni coating. Sohi et al. [33] discovered 13 wt% of Ni and Tian et al. [32] studied 6-15 wt% nickel of Zn–Ni coatings while using Zn as the anode. In this study, Zn anodes resulted in the highest Ni content in the coating, while stainless steel led to the lowest. These differences in Ni weight percentages are attributed to the electrochemical properties of the anode materials, which either facilitate or inhibit the deposition of Ni.

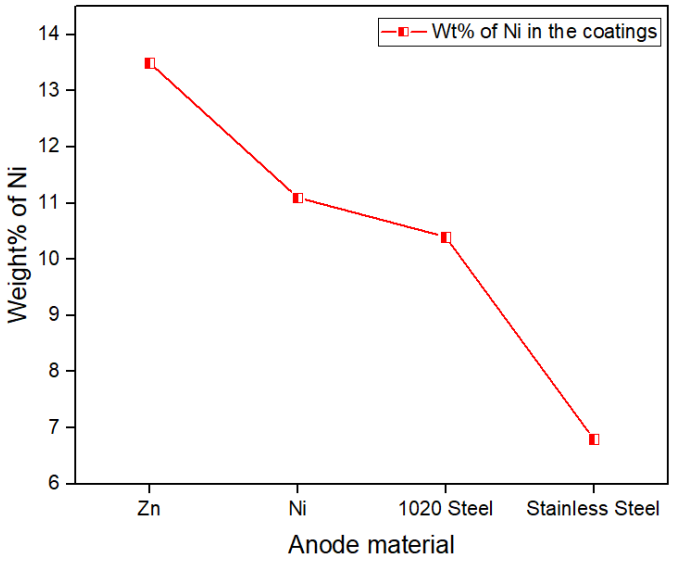

Figure 6. Percentage composition of Ni in Zn–Ni coatings tested by EDS Mapping using various anode materials.

In the electroplating process, a constant current was applied externally, ensuring the necessary electron flow for ion reduction at the cathode. Zinc anodes, while introducing Zn ions into the solution, support a continuous reduction process, resulting in higher Ni deposition rates. The additional Ni ions provided by the Ni anode contribute to maintaining a steady concentration of Ni in the electrolyte, facilitating consistent Ni deposition. However, the introduction of Fe ions from steel anodes creates competitive interactions with Ni ions in the electrolyte, which can inhibit the Ni deposition process and subsequently reduce the Ni content in the coating. For stainless steel anodes, the situation is more complex. The anodic polarization during the electroplating process disrupts the protective passive film on the stainless steel surface, leading to the formation of chromium ions. These chromium ions, along with Fe ions, are introduced into the electrolyte, where they compete with Ni ions for reduction at the cathode. This competition, coupled with the disruption of the passive film, significantly hinders the Ni deposition process, resulting in the lowest Ni content observed in coatings produced with stainless steel anodes.

3.4. Crystal Structure and Crystalline Size

The XRD peaks are shown in Figure 7a, which illustrates how different anode materials influence the phases present in Zn–Ni coatings. All samples show peaks corresponding to η-Zn and γ-Ni_5Zn_{21} phases, indicating that these are predominant phases in the Zn–Ni coatings regardless of the anode used. The intensity of the peak around 43° is the highest among all four curves. The sharp and intense peaks in the Zn anode coating pattern indicate a well-crystallised structure. It implies that regardless of the anode material, the preferred orientation is the γ- (330)/η- (101) plane. However, as the patterns are zoomed in from 35 to 50°, we can see the highest peaks (around 43°) are slightly shifted from one another. The reasons might be lattice strain and stress [34], phase composition, and crystallite size effects [35]. Lattice strain can cause a shift in the diffraction peaks. When atoms are displaced from their ideal positions due to stress or strain within the crystal

lattice, the interplanar spacing changes. Compressive stress typically shifts peaks to higher 2θ values, while tensile stress shifts peaks to lower 2θ values. Different anode materials can induce different levels of residual stress in the deposited Zn–Ni coatings, leading to peak shifts. Zn anode coating shows compressive stress whilst the coating using 1020 steel shows tensile stress. Scherrer broadening [36] suggests that smaller crystallite sizes can cause peak broadening and slight shifts due to increased surface energy effects. If the crystallite size varies significantly between samples deposited with different anode materials, it can contribute to peak shifts, as shown in Figure 7.

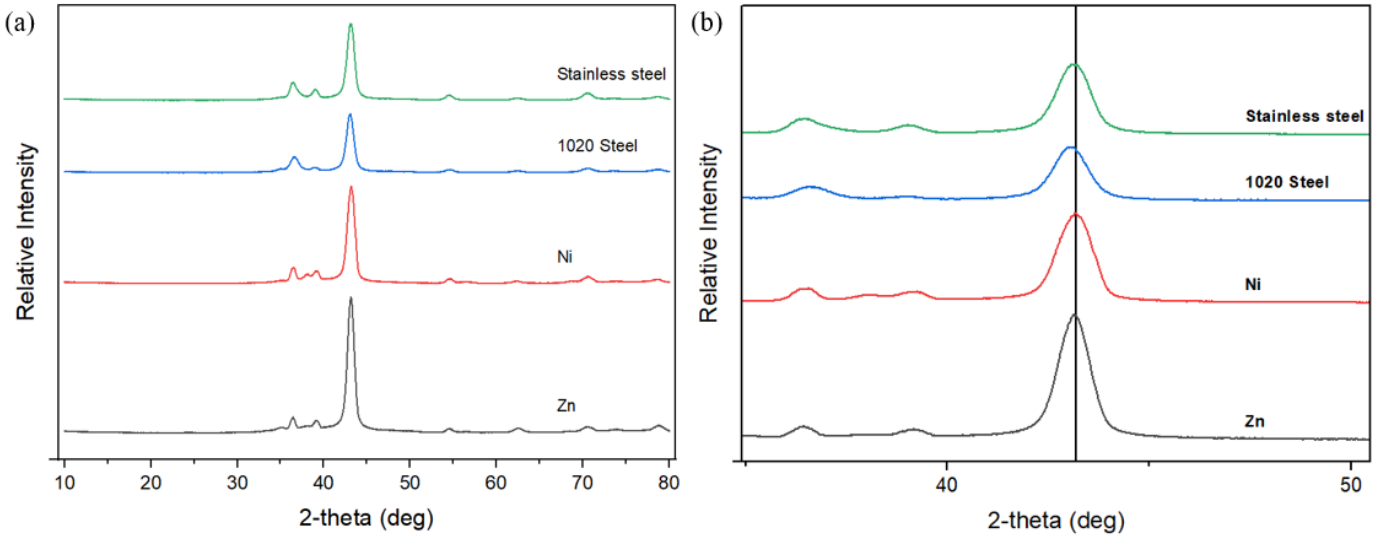

Figure 7. XRD patterns of Zn–Ni coatings deposited with Zn, Ni, 1020 steel, and stainless steel (**a**) in the ranges of 10~80°, (**b**) 35~50°.

Furthermore, the highest peak shows overlapping among the samples, which indicates that two different crystallographic planes have similar d-spacings and hence diffract X-rays at nearly the same angle (2θ), or show the presence of multiple phases or compounds in the coating, where some phases have planes with similar d-spacings [37]. When a straight line is drawn at 43° on the 2θ axis, it can be observed that the peak for the 1020 steel anode coating is centred on this line, effectively dividing the peak into two equal halves. In contrast, for the other three curves representing stainless steel, nickel, and zinc, the line intersects their peaks but is positioned more to the left of the peak centres, indicating a shift. This shift could imply a dominance of one phase over the other. Stainless steel anode coating has a higher γ phase concentration with little η phase contribution. This results in a broader peak slightly left of the centre. Ni and Zn anode coatings demonstrate a strong dominance of the η phase with a very sharp and significantly left-shifted peak, indicating minimal gamma phase presence. Therefore, the 1020 steel peak is centred at 43°, indicating balanced phases. Stainless steel shows a higher γ phase, while Ni and Zn have dominant η phases with left-shifted peaks. It can be concluded that the use of different anodes affects the phase composition and stress characteristics of Zn–Ni coatings.

The crystallite sizes of the coatings were measured through the Scherrer equation. Figure 8 illustrates the effect of anode material on the average size of nanocrystalline deposits. The crystallite size of Zn–Ni coatings varies slightly with the choice of anode material. The Zn anode leads to larger crystallites, while 1020 steel and 316 L stainless steel anodes result in finer particle structures due to the incorporation of Fe and other alloying elements. Larger crystallites suggest that the Zn anode promotes crystalline growth, possibly due to its relatively high atomic mobility [38], which facilitates recrystallisation. The crystalline size slightly decreases to around 9.0 nm with nickel as the anode material. Nickel has a face-centred cubic crystal structure, which might result in a slightly smaller crystalline size due to an increase in nucleation and growth rates compared to zinc [39]. The

crystalline size significantly decreases to less than 8.0 nm while using the 1020 steel anode. This might be due to the interaction between the carbon content in 1020 steel and the Zn–Ni coating process, leading to finer crystalline structures [40]. Grain refinement occurs because the carbon atoms can be incorporated into the grain boundaries, hindering the movement of dislocations and the growth of larger grains. stainless steel used as an anode could have a complex electrode potential as it contains chromium, nickel, and other alloying elements. The potential difference with stainless steel can vary significantly, impacting the electrochemical environment and deposition kinetics. This can lead to slight increases in crystalline size due to the specific interactions between the alloying elements and the deposition process.

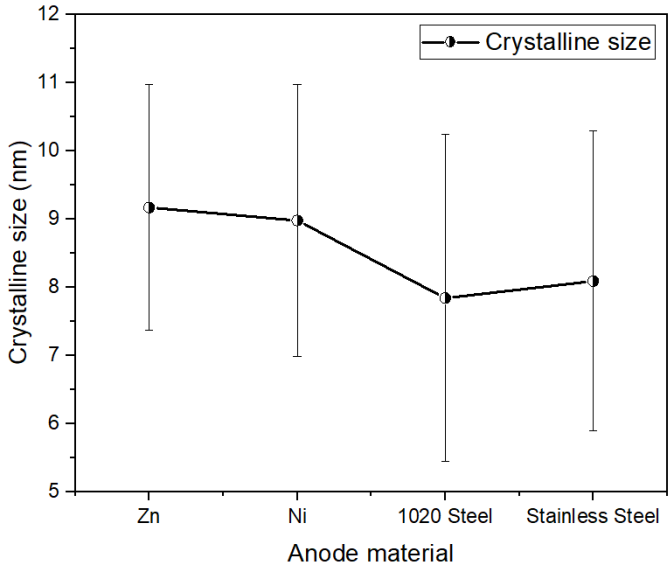

Figure 8. The effect of anode material on crystallite size.

The crystallite size of Zn–Ni coatings significantly influences their properties, with smaller crystallites generally enhancing corrosion resistance, hardness, adhesion, surface smoothness, and electrochemical activity. Smaller crystallite sizes create more grain boundaries, which act as barriers to corrosion and improve mechanical properties like hardness due to the Hall–Petch effect. They also promote better adhesion by conforming more closely to the substrate, resulting in a smoother surface finish and increased electrochemical performance by providing a larger active surface area. Conversely, larger crystallite sizes can lead to reduced corrosion resistance, lower hardness, poorer adhesion, rougher surfaces, and diminished electrochemical activity. Therefore, controlling the crystallite size through the selection of anode material, as shown in Figure 8, is crucial for optimizing the performance of Zn–Ni coatings for specific applications.

3.5. Microhardness

The microhardness of Zn–Ni alloy coatings electrodeposited at different conditions is shown in Figure 9. Before the microhardness tests, the samples were ground with silicon carbide papers (120 to 4000 grit), polished with diamond suspensions (6 µm to 1 µm), finished with 0.05 µm colloidal silica, and then cleaned with distilled water and ethanol before testing.

The microhardness values of Zn–Ni coatings are relatively consistent across different anode materials, staying within the range of 140 Hv to 210 Hv, whereas the hardness of Cd coatings was reported to be around 109 Hv, as studied by Ganesan et al. [41], and 81.6 Hv, as researched by Sriraman et al. [2]. The hardness of the Zn–Ni alloy coatings shows slight variations with different anode materials, all higher than that of Cd coatings. The highest hardness observed with Zn anodes can be attributed to higher Ni content, and possibly favourable residual stress states. As seen in Figure 3a, the Zn anode coating has

a much denser microstructure, which may lead to an increase in the hardness. The lower hardness with steel and 316 L stainless steel anodes may be due to reduced Ni content and the presence of other alloying elements. It may also be caused by the impurities introduced to the coatings, as shown in Figure 3c,d. This suggests that while the deposition parameters are crucial, the choice of anode material can fine-tune the mechanical properties of the coatings.

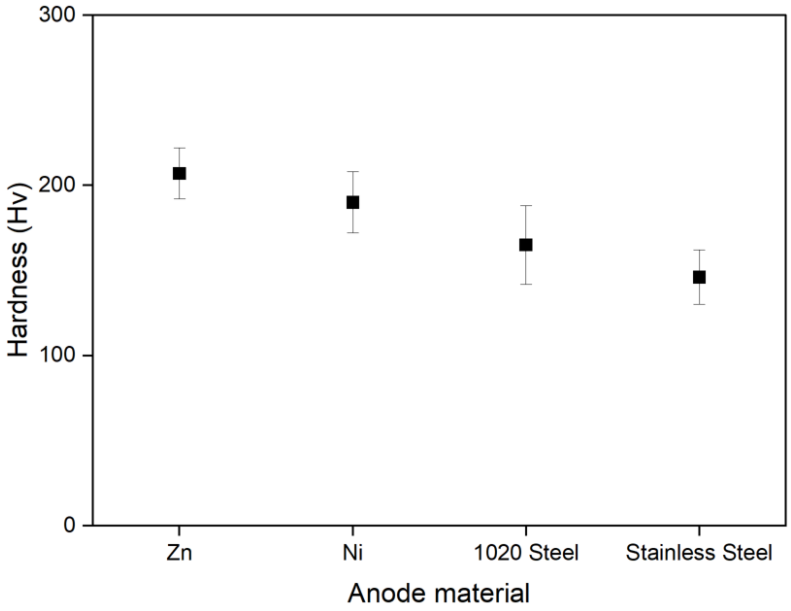

Figure 9. The effect of anode material on the hardness of the electrodeposited Zn–Ni alloy coatings.

3.6. Electrochemical Studies

The potentiodynamic polarisation curves for Zn–Ni alloy nanocrystalline coatings using different anodes on 1020 steel using a 3.5 wt% NaCl solution are shown in Figure 10. The use of a 3.5 wt% NaCl solution is justified as it effectively simulates marine environments and provides a consistent medium for evaluating the electrochemical and protective properties of coatings, ensuring the relevance of our findings to both research and industry. The electrochemical parameters (E_{corr}, i_{corr}) for Zn–Ni alloy coatings are summarised in Table 2.

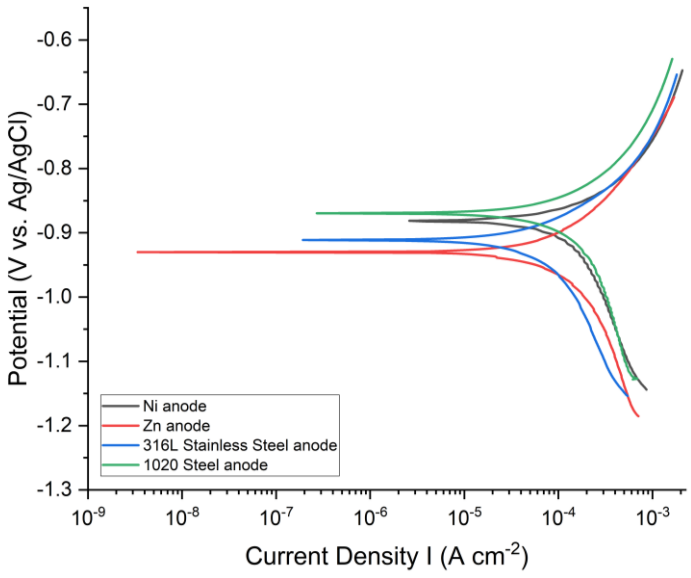

Figure 10. Polarisation curve for Zn–Ni alloy coatings deposited using different anode materials.

Table 2. The electrochemical parameters (E_{corr}, i_{corr}) of coating samples in a 3.5 wt% NaCl solution.

Anode Material Used	E_{corr} (V)	βa (V)	βc (V)	I_{corr} (μA/cm^2)	Corrosion Rate (mm/year)
Zn	−0.977	0.084	0.141	30	0.439
Ni	−0.880	0.113	0.229	105	1.538
1020 Steel	−0.872	0.097	0.158	70	1.025
316 L Stainless steel	−0.912	0.088	0.171	43	0.629

The corrosion potentials of all deposits remain negative compared to those of 1020 steel and Cd coatings, with potentials around −0.44 V and −0.76 V, respectively, reported by Conde et al. [20], which means that all deposits can provide corrosion protection to the 1020 steel and the Zn–Ni coatings show better corrosion behaviour than cadmium coatings. The corrosion potential of Zn–Ni coatings using 1020 steel anode show the highest corrosion potential, indicating it has more resistance to corrosion compared to the coatings using other anode materials. However, the high corrosion current density suggests a higher rate of metal dissolution, which may be due to the lack of formation of a protective passive layer. The Zn anode coating, despite a more negative corrosion potential, shows a lower corrosion current density, indicating effective sacrificial protection with a slower corrosion rate, making it more susceptible to galvanic corrosion. Its corrosion current density is similar to Conde et al. [20] and Tozar et al. [42], which ranges from about 20 to 30 μA/cm^2 and 7 to 45 μA/cm^2 for Zn–Ni coatings. The low corrosion current density suggests a slow rate of corrosion, possibly due to the formation of stable corrosion products. Ni and 316 L stainless steel anode coatings show intermediate behaviour specifically for the corrosion potential. The Zn–Ni coating using a Zn anode appears to have the lowest corrosion rate of 0.439 mm/year, and the coating using a Ni anode has the highest corrosion rate of 1.538 mm/year. The polarization corrosion studies in a neutral solution of sodium chloride showed comparable outcomes, with corrosion rates measured as 0.5 mm/year for Zn–Ni and 1.24 mm/year for Zn [43]. Li et al. [44] conducted the corrosion tests with the result of Zn–Ni coatings with a corrosion rate of approximately 0.94 mm/year, similar to the results from this research.

The relationship between crystallite size, current density in corrosion, and Ni content in Zn–Ni coatings is critical in determining their corrosion resistance. Smaller crystallite sizes, particularly those under 8 nm, as observed with 1020 steel anodes, enhance corrosion resistance by increasing grain boundary density, thereby impeding corrosion pathways. In contrast, larger crystallite sizes, around 9–10 nm, associated with Zn anodes, may reduce corrosion resistance. The influence of current density during electrodeposition is also significant: lower current densities generally promote finer microstructures, leading to improved corrosion performance. For example, Zn anodes, which exhibit lower corrosion current densities of approximately 30 μA/cm^2, correspond to slower corrosion rates, measured at 0.44 mm/year. Ni content further modulates corrosion resistance, with an optimal range around 13.5 wt% Ni, as seen with Zn anode coatings, which enhances the formation of corrosion-resistant γ-Ni_5Zn_{21} phases. However, Ni contents exceeding 25–30 wt% may compromise sacrificial protection by shifting the coating's reliance from sacrificial action to barrier properties [16]. Variations in these results arise from the complex interplay between crystallite size, current density, and Ni content, where adjustments in one parameter can lead to significant changes in corrosion behaviour. This underscores the necessity for precise control of deposition parameters to optimise the corrosion resistance of Zn–Ni coatings.

4. Conclusions

This study presents novel insights into the effects of different anode materials on Zn–Ni alloy coatings, emphasizing the importance of anode selection in optimizing coating properties. It highlights the significant influence of anode material on the quality and properties of Zn–Ni coatings, revealing that Zn anodes offer consistent and efficient coating processes, while Ni, 1020 steel, and 316 L stainless steel exhibit inefficiencies. Voltage

analysis showed that Zn anodes maintained the lowest and most stable voltage (~0.5 V), leading to smoother, more homogeneous coatings with minimal defects and a fine platelet structure less than 1 µm in size. Cross-sectional analysis confirmed that Zn anodes produced uniform coatings with a thickness of 14.5 µm, while stainless steel anodes, though yielding thicker coatings (33 µm), introduced significant porosity and defects. Coatings deposited using a nickel anode demonstrated excellent interface properties, exhibiting strong adhesion to the substrate and consistent interface quality. Phase composition analysis showed that Zn anodes provided the highest Ni content (13.5 wt%), enhancing corrosion resistance, whereas steel anodes resulted in lower Ni content (7 wt%) and more defects. Microhardness tests demonstrated that Zn anodes achieved the highest hardness (~210 Hv), with stainless steel anodes producing the lowest (~140 Hv). Electrochemical studies further affirmed the superiority of Zn anodes, showing a low corrosion rate of 0.44 mm/year. In summary, Zn anodes are ideal for achieving high-quality, corrosion-resistant Zn–Ni coatings, making them a safer and more effective alternative to cadmium coatings. Ni anodes offer acceptable quality but with superior adhesion to substrates, while 1020 steel and 316 L stainless steel may be considered for cost-sensitive applications with increased defect tolerance.

Author Contributions: Methodology, L.Y.; Formal analysis, L.Y.; Writing—original draft, L.Y.; Writing—review & editing, L.Y., S.W. and R.J.K.W.; Supervision, S.W. and R.J.K.W. All authors have read and agreed to the published version of the manuscript.

Funding: This research received no external funding.

Institutional Review Board Statement: Not applicable.

Informed Consent Statement: Not applicable.

Data Availability Statement: Data is contained within the article.

Conflicts of Interest: The authors declare no conflict of interest.

References

1. Baldwin, K.R.; Smith, C.J.E. Advances in Replacements for Cadmium Plating in Aerospace Applications. *Trans. IMF* **1996**, *74*, 202–209. [CrossRef]
2. Sriraman, K.R.; Strauss, H.W.; Brahimi, S.; Chromik, R.R.; Szpunar, J.A.; Osborne, J.H.; Yue, S. Tribological behavior of electrodeposited Zn, Zn–Ni, Cd and Cd–Ti coatings on low carbon steel substrates. *Tribol. Int.* **2012**, *56*, 107–120. [CrossRef]
3. Charkiewicz, A.E.; Omeljaniuk, W.J.; Nowak, K.; Garley, M.; Nikliński, J. Cadmium Toxicity and Health Effects—A Brief Summary. *Molecules* **2023**, *28*, 6620. [CrossRef] [PubMed]
4. Wang, M.; Chen, Z.; Song, W.; Hong, D.; Huang, L.; Li, Y. A review on Cadmium Exposure in the Population and Intervention Strategies Against Cadmium Toxicity. *Bull. Environ. Contam. Toxicol.* **2021**, *106*, 65–74. [CrossRef]
5. Fernandes, M.F.; dos Santos, J.R.M.; de Oliveira Velloso, V.M.; Voorwald, H.J.C. AISI 4140 Steel Fatigue Performance: Cd Replacement by Electroplated Zn-Ni Alloy Coating. *J. Mater. Eng. Perform.* **2020**, *29*, 1567–1578. [CrossRef]
6. Mosavat, S.; Bahrololoom, M.; Shariat, M. Electrodeposition of nanocrystalline Zn–Ni alloy from alkaline glycinate bath containing saccharin as additive. *Appl. Surf. Sci.* **2011**, *257*, 8311–8316. [CrossRef]
7. Ghaziof, S.; Gao, W. Electrodeposition of single gamma phased Zn–Ni alloy coatings from additive-free acidic bath. *Appl. Surf. Sci.* **2014**, *311*, 635–642. [CrossRef]
8. Oladijo, O.; Mathabatha, M.; Popoola, A.; Ntsoane, T. Characterization and corrosion behaviour of plasma sprayed Zn-Sn alloy coating on mild steel. *Surf. Coat. Technol.* **2018**, *352*, 654–661. [CrossRef]
9. Lodhi, Z.F.; Tichelaar, F.D.; Kwakernaak, C.; Mol, J.M.C.; Terryn, H.; de Wit, J.H.W. A combined composition and morphology study of electrodeposited Zn–Co and Zn–Co–Fe alloy coatings. *Surf. Coat. Technol.* **2008**, *202*, 2755–2764. [CrossRef]
10. Hegde, A.; Venkatakrishna, K.; Eliaz, N. Electrodeposition of Zn–Ni, Zn–Fe and Zn–Ni–Fe alloys. *Surf. Coat. Technol.* **2010**, *205*, 2031–2041. [CrossRef]
11. Karahan, I.H.; Güder, H.S. Electrodeposition and properties of Zn, Zn–Ni, Zn–Fe and Zn–Fe–Ni alloys from acidic chloride–sulphate electrolytes. *Trans. IMF* **2009**, *87*, 155–158. [CrossRef]
12. Maniam, K.K.; Paul, S. Corrosion Performance of Electrodeposited Zinc and Zinc-Alloy Coatings in Marine Environment. *Corros. Mater. Degrad.* **2021**, *2*, 163–189. [CrossRef]
13. Nakano, H.; Arakawa, S.; Oue, S.; Kobayashi, S. Electrodeposition Behavior of Zn–Fe Alloy from Zincate Solution Containing Triethanolamine. *Mater. Trans.* **2015**, *56*, 1664–1669. [CrossRef]

14. Gerhátová, Ž.; Babincová, P.; Drienovský, M.; Pašák, M.; Černičková, I.; Ďuriška, L.; Havlík, R.; Palcut, M. Microstructure and Corrosion Behavior of Sn–Zn Alloys. *Materials* **2022**, *15*, 7210. [CrossRef] [PubMed]
15. Byk, T.; Gaevskaya, T.; Tsybulskaya, L. Effect of electrodeposition conditions on the composition, microstructure, and corrosion resistance of Zn–Ni alloy coatings. *Surf. Coat. Technol.* **2008**, *202*, 5817–5823. [CrossRef]
16. MS, C.; Srinivasan, S.; Pushpavanam, M. Properties of Zinc alloy electrodeposits produced from acid and alkaline electrolytes. *J. Solid State Electrochem.* **2009**, *13*, 781–789.
17. Farooq, A.; Ahmad, S.; Hamad, K.; Deen, K.M. Effect of Ni Concentration on the Surface Morphology and Corrosion Behavior of Zn-Ni Alloy Coatings. *Metals* **2022**, *12*, 96. [CrossRef]
18. Boonyongmaneerat, Y.; Saenapitak, S.; Saengkiettiyut, K. Reverse pulse electrodeposition of Zn–Ni alloys from a chloride bath. *J. Alloys Compd.* **2009**, *487*, 479–482. [CrossRef]
19. Abou-Krisha, M.M.; Assaf, F.H.; Toghan, A.A. Electrodeposition of Zn–Ni alloys from sulfate bath. *J. Solid State Electrochem.* **2007**, *11*, 244–252. [CrossRef]
20. Conde, A.; Arenas, M.; de Damborenea, J. Electrodeposition of Zn–Ni coatings as Cd replacement for corrosion protection of high strength steel. *Corros. Sci.* **2011**, *53*, 1489–1497. [CrossRef]
21. Feng, Z.; An, M.; Ren, L.; Zhang, J.; Yang, P.; Chen, Z. Corrosion mechanism of nanocrystalline Zn-Ni alloys as replacement of Zn and Cd coatings in a new DMH-based bath. *RSC Adv.* **2016**, *6*, 64726–64740. [CrossRef]
22. Mosavat, S.; Shariat, M.; Bahrololoom, M. Study of corrosion performance of electrodeposited nanocrystalline Zn–Ni alloy coatings. *Corros. Sci.* **2012**, *59*, 81–87. [CrossRef]
23. Gnanamuthu, R.M.; Mohan, S.; Saravanan, G.; Lee, C.W. Comparative study on structure, corrosion and hardness of Zn–Ni alloy deposition on AISI 347 steel aircraft material. *J. Alloys Compd.* **2012**, *513*, 449–454. [CrossRef]
24. Sadananda, K.; Yang, J.H.; Iyyer, N.; Phan, N.; Rahman, A. Sacrificial Zn–Ni coatings by electroplating and hydrogen embrittlement of high-strength steels. *Corros. Rev.* **2021**, *39*, 487–517. [CrossRef]
25. Park, H.; Szpunar, J.A. The Microstructural Characterization of Electrogalvanized Zinc–Iron and Zinc–Nickel Coatings. *Texture Stress Microstruct.* **2000**, *34*, 579539.
26. Ciszewski, A.; Posluszny, S.; Milczarek, G.; Baraniak, M. Effects of saccharin and quaternary ammonium chlorides on the electrodeposition of nickel from a Watts-type electrolyte. *Surf. Coatings Technol.* **2004**, *183*, 127–133. [CrossRef]
27. Hughes, N. LHE Zn-Ni Corrosion Testing and Implications for Fasteners. 2022. Available online: https://www.zn-ni.com/docs/Zinc%20Nickel%20Corrosion%20Testing%202-2022.pdf (accessed on 1 February 2022).
28. Thangaraj, V.; Hegde, A. Electrodeposition and compositional behaviour of Zn-Ni alloy. *Indian J. Chem. Technol.* **2007**, *14*, 246–252.
29. Tafreshi, M.; Allahkaram, S.R.; Mahdavi, S. Effect of PTFE on characteristics, corrosion, and tribological behavior of Zn–Ni electrodeposits. *Surf. Topogr. Metrol. Prop.* **2020**, *8*, 045013. [CrossRef]
30. Lindley, P.; Moss, D. Elements of X-ray crystallography by L. V. Azaroff. *Acta Crystallogr. Sect. A* **1970**, *26*, 701. [CrossRef]
31. Lotfi, N.; Aliofkhazraei, M.; Rahmani, H.; Darband, G.B. Zinc–Nickel Alloy Electrodeposition: Characterization, Properties, Multilayers and Composites. *Prot. Met. Phys. Chem. Surf.* **2018**, *54*, 1102–1140. [CrossRef]
32. Tian, W.; Xie, F.Q.; Wu, X.Q.; Yang, Z.Z. Study on corrosion resistance of electroplating zinc–nickel alloy coatings. *Surf. Interface Anal.* **2009**, *41*, 251–254. [CrossRef]
33. Sohi, M.H.; Jalali, M. Study of the corrosion properties of zinc–nickel alloy electrodeposits before and after chromating. *J. Mech. Work. Technol.* **2003**, *138*, 63–66.
34. Jiang, W.; Peacor, D.R.; Árkai, P.; Tóth, M.; Kim, J.W. TEM and XRD determination of crystallite size and lattice strain as a function of illite crystallinity in pelitic rocks. *J. Metamorph. Geol.* **1997**, *15*, 267–281. [CrossRef]
35. Hassanzadeh-Tabrizi, S. Precise calculation of crystallite size of nanomaterials: A review. *J. Alloys Compd.* **2023**, *968*, 171914. [CrossRef]
36. Patterson, A.L. The Scherrer formula for X-ray particle size determination. *Phys. Rev. B* **1939**, *56*, 978–982. [CrossRef]
37. Khan, H.; Yerramilli, A.S.; D'Oliveira, A.; Alford, T.L.; Boffito, D.C.; Patience, G.S. Experimental methods in chemical engineering: X-ray diffraction spectroscopy—XRD. *Can. J. Chem. Eng.* **2020**, *98*, 1255–1266. [CrossRef]
38. Cui, S.; Du, Y.; Zhang, L.; Liu, Y.; Xu, H. Assessment of atomic mobilities in fcc Al-Zn and Ni-Zn alloys. *Calphad* **2010**, *34*, 446–451. [CrossRef]
39. Anwar, S.; Zhang, Y.; Khan, F. Electrochemical behaviour and analysis of Zn and Zn–Ni alloy anti-corrosive coatings deposited from citrate baths. *RSC Adv.* **2018**, *8*, 28861–28873. [CrossRef]
40. Jones, R.H.E. *Environmental Effects on Engineered Materials*, 1st ed.; CRC Press: Boca Raton, FL, USA, 2001.
41. Ganesan, P.; Kumaraguru, S.P.; Popov, B.N. Development of compositionally modulated multilayer Zn–Ni deposits as replacement for cadmium. *Surf. Coatings Technol.* **2007**, *201*, 7896–7904. [CrossRef]
42. Tozar, A.; Karahan, I. Structural and corrosion protection properties of electrochemically deposited nano-sized Zn–Ni alloy coatings. *Appl. Surf. Sci.* **2014**, *318*, 15–23. [CrossRef]

43. Kim, H.; Popov, B.N.; Chen, K.S. Comparison of corrosion-resistance and hydrogen permeation properties of Zn–Ni, Zn–Ni–Cd and Cd coatings on low-carbon steel. *Corros. Sci.* **2003**, *45*, 1505–1521. [CrossRef]
44. Li, S.; Song, G.; Zhang, Y.; Fu, Q.; Pan, C. Graphene-Reinforced Zn–Ni Alloy Composite Coating on Iron Substrates by Pulsed Reverse Electrodeposition and Its High Corrosion Resistance. *ACS Omega* **2021**, *6*, 13728–13741. [CrossRef] [PubMed]